ELSEVIER

Polymer 43 (2002) 1473–1481

polymer

www.elsevier.com/locate/polymer

Second-order phase transition of high isotactic polypropylene at high temperature

Fangming Gu[a], Masamichi Hikosaka[b,*], Akihiko Toda[b], Swapan Kumar Ghosh[b], Shinichi Yamazaki[a], Motoki Arakaki[b], Koji Yamada[c]

[a]*Venture Business Laboratory, Hiroshima University, 2-313 Kagamiyama, Higashi Hiroshima 739-8527, Japan*
[b]*Faculty of Integrated Arts and Science, Hiroshima University, 1-7-1 Kagamiyama, Higashi Hiroshima 739-8521, Japan*
[c]*Oita Research Center, Sunallomer Ltd, 2 Nakanosu, Oita 870-0189, Japan*

Received 18 April 2001; received in revised form 24 July 2001; accepted 14 August 2001

Abstract

A second-order phase transition of α2 form isotactic polypropylene (iPP) is found at high annealing temperature (T_a = 159.3 °C) by means of X-ray diffraction method. Although the lattice shape and the space group keep the same as those of the α2 form, i.e. monoclinic and $P2_1/c$, with increase of T_a, it has been revealed that there are discontinuous increases in the slopes of the lattice constants a and b against T_a plots, while the c and the β keep almost constant. As a result, the slope of the unit cell volume V versus T_a plot also shows a discontinuous increase at T_a = 159.3 °C, indicating the occurrence of the second-order phase transition. In order to distinguish the two phases, the phase above the transition temperature is named α2′ phase and the transition temperature is denoted $T_{\alpha 2-\alpha 2'}$. These facts suggested that the α2′ form is a mobile phase where the molecular chains would become loosely packed and mobile, promoting the better chain sliding diffusion. A fast lamellar thickening process has been confirmed in the higher temperature region than $T_{\alpha 2-\alpha 2'}$, which was reported in the precedent paper. General significance is proposed that mobile phases possibly exist at high temperature, close to the melting temperature and accelerate lamellar thickening, which improves physical properties of polymers. © 2001 Published by Elsevier Science Ltd.

Keywords: Isotactic polypropylene; Second-order phase transition; Mobile phase

1. Introduction

Since the application of Ziegler–Natta catalyst technology, the structure, morphology and physical properties of isotactic polypropylene (iPP) have been extensively examined for the past several decades. In the crystalline state, it has long been recognized that the iPP can exhibit several different crystalline forms, namely the monoclinic (α) form (including α1 and α2) [1–13], the trigonal (β) form [14–19], the triclinic (γ) form [20–26] and the mesomorphic (smectic) form [27]. The formation and their mutual phase transitions are critically dependent on the crystallization conditions, the molecular weight and the tacticity [28].

When the iPP is cooled down from the melt or the solution, it crystallizes usually into α form [1,2]. The crystal structure of the α form is built up of isomorphous 3_1 helices disposed in layers parallel to the *ac* plane. Since the presence of the asymmetrically substituted methyl groups causes rotation around the backbone bonds to be direction-dependent, the corresponding helical conformation in the crystalline state can be formed by either right or left-handed rotation about the central axis. Independent of the handiness, the helix also has unique 'up' and 'down' directions with respect to the positions of those methyl groups [3–7]. Therefore, there are four distinguishable chain shapes in the crystallographic unit cell. Natta and Corradini proposed a monoclinic unit cell in the space groups of $C2/c$ and Cc [1]. However, in this structure, statistical disorder with respect to the up and down position of methyl group of the chain is present. Later, Mencik [3] and Hikosaka and Seto [4] described the structure of the α form of iPP in terms of two limiting modifications, α1 and α2, respectively. The α1 form has a statistical disorder like that described for the space group $C2/c$. The α2 form is an ordered phase characterized by regularity of the up and down position of the methyl group along the chain, as in the space group $P2_1/c$. The α1–α2 transition is observed upon annealing in the high temperature region, where 'wrong' chains in $C2/c$ should be exchanged with 'correct chains' by exchanging vertically to the chain axis [4].

Naturally, it is expected that the isotacticity (relating to

* Corresponding author. Tel.: +81-824-24-6548; fax: +81-824-24-2652.
E-mail address: hikosaka@hiroshima-u.ac.jp (M. Hikosaka).

0032-3861/02/$ - see front matter © 2001 Published by Elsevier Science Ltd.
PII: S0032-3861(01)00667-X

defect along the chain) will play an important role during the $\alpha1 \rightarrow \alpha2$ transition. Only very recently it has become possible to obtain the iPP with very high isotacticity (the pentad content [mmmm] > 99.5%). In fact, it has been revealed that the crystal lattice constants, crystallinity, apparent crystal size and lamellar thickness are all dependent on isotacticity and crystallization temperature [8–10]. When the high isotactic material is crystallized or annealed in the high temperature region ever reached, it yields the two important findings. One is that the fraction of $\alpha2$ can be made to approach unity [11]. The other is the complete absence of the cross-hatching. This challenges the previous 'consensus' that the cross-hatching should be always characteristic of the morphology of the α form of iPP [12]. Accordingly, the spherulite or the axialite produced in the high temperature region will be fully occupied by the radial lamellae only [13].

For linear polymers, it has been generally expected that molecular chains would become much more mobile at high temperature. In some cases, 'mobile phases', such as the hexagonal phase and the liquid crystalline phase, can be observed [29–31]. This could give rise to significant lamellar thickening, as predicted by chain sliding diffusion theory proposed by one of the authors (MH) [32,33], which significantly improves physical properties, such as melting temperature (T_m), mechanical properties and so on. In the case of iPP, it is not sure whether a mobile phase exists or not at small ΔT. The well-established $\alpha1-\alpha2$ structure change cannot be realized without the transformation from the immobile state at lower temperature to the mobile state at high temperature, because for $\alpha1-\alpha2$ transformation, 'wrong chains' should be exchanged vertically to the chain axis. In our previous study, the iPP with a very high isotacticity (99.6%) enabled the high temperature crystallization, i.e. crystallization at a low ΔT, which results in the significant increase of melting temperature higher than 180 °C [34]. This also suggests that a mobile phase of iPP exists at high T_a. Therefore, it is of value to confirm existence of a new mobile phase of iPP at high T_a not only for understanding the above general structure and morphology of polymer materials but also for exploring a relationship between chain mobility and their mechanical properties.

The purpose of this work is to explore whether there exists a 'mobile phase' for high isotactic iPP at high temperature and how it relates to improvements on the structure and morphology.

2. Experimental section

2.1. Sample preparation

The isotactic polypropylene (iPP) supplied by Sunallomer Ltd has molecular weight $M_w = 64 \times 10^3$ and $M_w/M_n = 2.4$, as measured by gel permeation chromatography (GPC). The percentage of isotacticity was determined to be 99.6% on the basis of pentad sequences [mmmm] using high-resolution ^{13}C nuclear magnetic resonance (^{13}C-NMR). It is proper to note here that the iPP, which was synthesized with the $MgCl_2$-supported catalyst, has only meso or racemic sequences and no head-to-head or 1,3-combination. Therefore, the possible stereo-defect is only the opposite insertion of monomers.

Small amount of the iPP was first sandwiched between two glass slides. The thickness of the polymer was controlled to be 0.2 mm by inserting metal spacers. In order to avoid the oxidation or degradation at high temperature for long hours' crystallization, the sample was sealed in a glass tube under vacuum. The whole glass tube along with the sample was held at 220 °C in an oil bath for 5 min to ensure the complete destruction of any crystalline remnants (the equilibrium temperature $T_m^0 \approx 186$ °C [36]). After that, they were rapidly transferred to another oil bath that was preset to 164 °C to allow an isothermal crystallization for 28 days and then quenched in frozen acetone.

Applying such long hours of isothermal crystallization at high temperature, the sample was completely solidified and very big spherulites (mm-order in size) were produced. One of the big spherulites was picked up and carefully cut along its radial direction into the rectangular shape with the width 0.2 mm, as shown in Fig. 1(a). Note that the cutting direction is also parallel to the a^* crystallographic direction [12,13], which will be confirmed in the related part of this study (Section 3.1). Fig. 1(b) schematically illustrates the cutting traces and the geometrical shape of the resulting sample.

2.2. X-ray instrumental

After cutting, the sample was mounted on the goniometer and rotating with its radial axis (a^* direction). The diameter of the collimator is 0.3 mm. The height of the sample was precisely adjusted to let the X-ray incident beam (actually normal to the a^* direction) pass through only the tip of the spherulite, also shown in Fig. 1(b).

Wide angle X-ray diffraction (WAXD) experiments were conducted with Rigaku's Rint 2100 X-ray generator. The X-ray beam was Cu Kα radiation from a rotating anode generator. The beam was monochromatized using a graphite crystal. During exposure, the sample was held at various temperatures for annealing with a blowing heater (Rigaku Denki Co., Ltd) under a running stream of hot nitrogen gas. A type K (CA) thermocouple was put very close to the sample, and a digital programmable controller (Chino Co., Ltd, KP1000), and hence obtained the temperature. The X-ray diffraction pattern was recorded on the imaging plate with the highest resolution of 25 μm so far (Fuji Photo Film Co., Ltd, FDL-IP UR-V). Utilizing a specially designed imaging plate reader (Rigaku Denki Co., Ltd, R-AXIS DS3), the digitized image was obtained and analyzed using the software (Rigaku Denki Co., Ltd, R-AXIS Display: Fiber Data Processing) developed by us

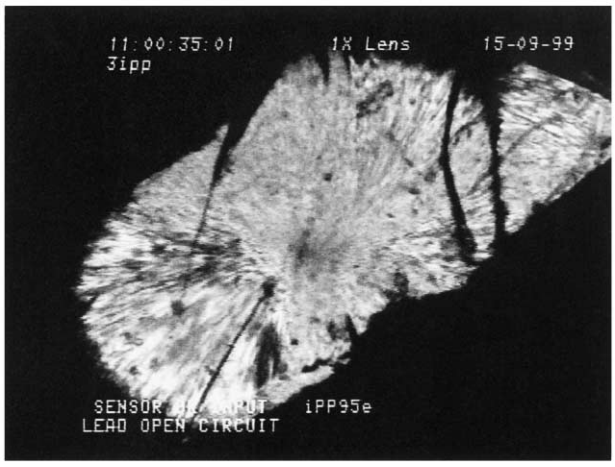

(a)

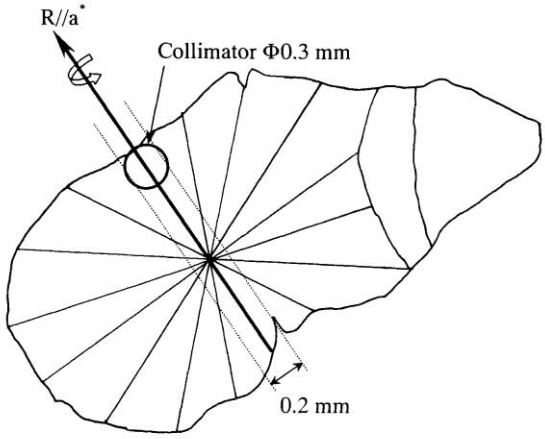

(b)

Fig. 1. (a) Optical micrograph and (b) schematic illustration of a typical big spherulite crystallized at $T_c = 163$ °C for 102 days. The scale bar indicates 0.5 mm. The dotted lines in the illustration represent the cutting traces.

and Rigaku Denki Co., Ltd. The camera length was calibrated with the fine Silicon powder pressed on the surface of the iPP sample every time.

2.3. 'Fiber data processing' method: space group determination

The I–2θ profiles were obtained by the newly developed software entitled 'Rigaku-Display: Fiber Data Processing'. Fig. 2 shows a typical analyzing menu. A simple description was given as follows. First, the incident beam center was determined using the double-ring method. Assuming the equatorial line is 0 layer, the height (Z) of each layer line was then obtained based on the estimation of the fiber period. The integration width (ΔZ) was defined by the upper or lower part of each arc (or spot in the case of better oriented sample). After that, the X-ray intensity for each reflection was integrated along the arc within this width in the different layer line. The peaks on the I–2θ profile were resolved using a curve resolution program.

2.4. Lattice constants measurement

In the case of lattice constants determination, the five strongest reflections, namely 110, 040, 130, 111 and $\bar{1}31$, are used to calculate the lattice constants by integration along the whole Debye–Scherrer ring. The lattice constant b is solely determined by the spacing of the 040 reflection; the lattice constants a, c and β are determined by the spacing of other four reflections. It should be noted here that the actual relative resolution of lattice spacing $\Delta d/d$ due to the limited resolution of the imaging plate (25 μm) become less than 5×10^{-2}% for 040 and 4×10^{-2}% for 130 when the camera length is 80 mm. For the purpose of lattice constants determination, the error is sufficiently small in this study.

3. Results

3.1. Image fiber pattern

Fig. 3 shows a typical X-ray image pattern obtained at room temperature. Since the illuminated area by the incident X-ray beam (0.3 mm in diameter) is comparatively small with respect to the large size of the spherulite (several mm in order), the sample should be well oriented within that limited area. Actually, all the concentrated rings have indeed degenerated into the elongated arcs, as shown in Figs. 2 and 3. Therefore, the pattern can be regarded as a kind of fiber pattern. Note that the fiber axis is in the a^* direction since the radial direction of the α form of iPP is known to be parallel to the a^* axis. Different layer lines (corresponding to $h = 0, \pm1, \pm2, \ldots$) can be easily distinguished in both Figs. 2 and 3. The detailed recognition and analysis on the image pattern will be given in Section 3.2. Nevertheless, such an image pattern directly confirmed that the sample was cut along its radial direction for a certainty.

Based on Fig. 2, we could index all the possible reflections and hence determine the space group. While on the basis of Fig. 3, we focus the attention only on the five strongest reflections, i.e. 110, 040, 130, 111 and $\bar{1}31$. It should be noted that the camera length used in Fig. 3 is twice as large as the one used in Fig. 2. In this way, the measurement precision will also be improved two times. Therefore, the lattice spacing and lattice constants will be determined or calculated using Fig. 3.

3.2. Extinction rule and space group

Figs. 4–6 show I–2θ fiber patterns corresponding to $h =$ 0, 1 and 2 layers at RT and $T_a = 166$ °C, respectively.

The well-crystallized sample at room temperature can be identified to be the α2 form. As described in the earlier

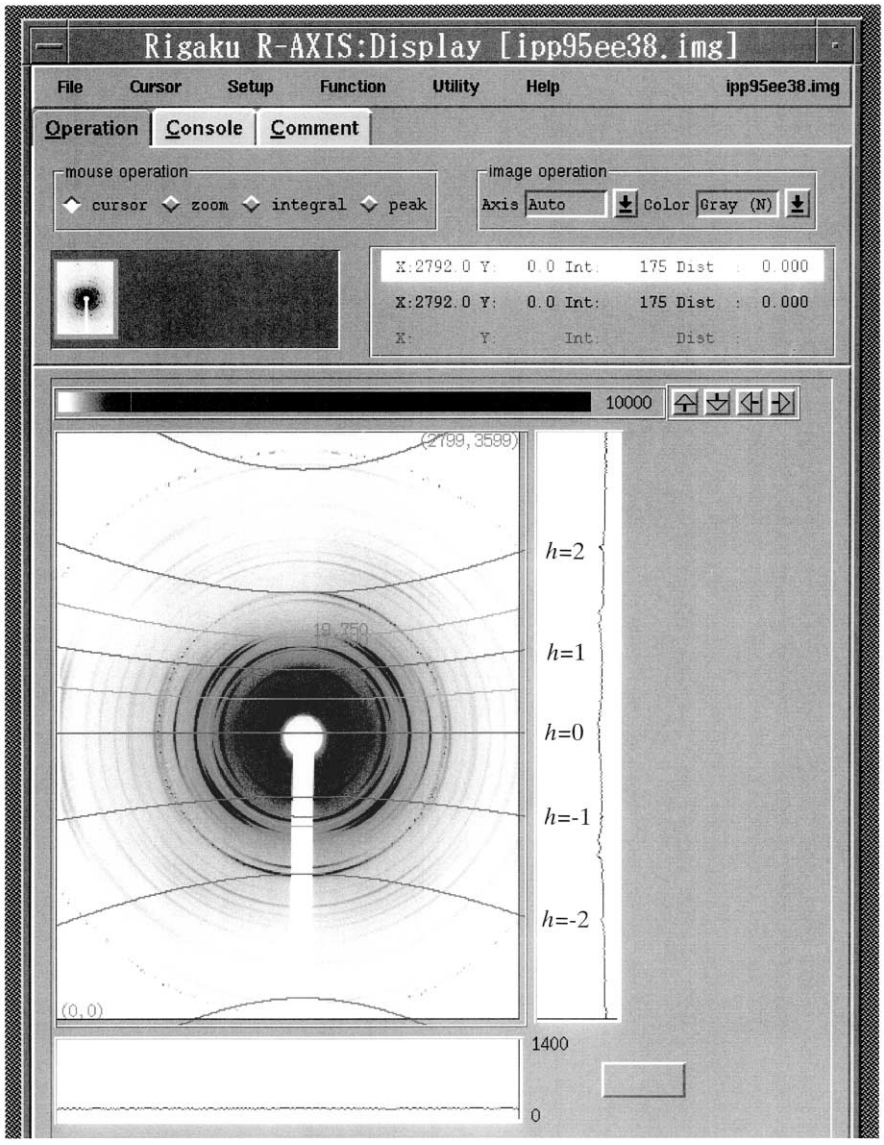

Fig. 2. A typical analyzing menu of the 'fiber data processing' method. X-ray diffraction pattern recorded by the imaging plate with the highest resolution of 25 μm. Different layer lines corresponding to $h = 0, \pm1, \pm2$, respectively, are shown on the image.

papers [4], the two modifications α1 and α2 have similar X-ray patterns for the reflections *hkl* with $h + k =$ even, whereas the reflections *hkl* with $h + k =$ odd are systematically absent in the α1 form owing to the extinction rule. In particular, the appearance of the reflections $\bar{1}61/\bar{2}31$ is often regarded as one of the main criteria to distinguish the α2 form from its α1 counterpart. Since the two reflections have almost the same lattice spacing, the two reflections are always superimposed in both the powder diffraction pattern and the *c*-axis oriented fiber pattern ($l = 1$). For long years, the structure factors of the two reflections have not been evaluated independently. However, in the present paper, it is seen that the two reflections are well separated. In addition, we also see that their reflection intensities are very similar, which means the structure factor $F_c(\bar{1}61) \approx F_c(\bar{2}31)$. This is in good agreement with the atomic model proposed by Hikosaka and Seto, 30 years ago [4].

Nevertheless, it should be noted that the two sets of fiber patterns at RT and at $T_a = 166\,^{\circ}C$ are very similar in appearance. We thus have good reason for assuming that the structure at high temperature has the same lattice shape, i.e. the monoclinic, as the α2 form. It was found that both $\bar{1}61$ and $\bar{2}31$ reflections are also present in the X-ray fiber patterns obtained at $T_a = 166\,^{\circ}C$.

After obtaining the lattice constants at the two annealing temperatures, all reflections in both sets of figures were indexed. Some of them are shown in Figs. 4–6. It has been confirmed again that the above two fiber patterns can be indexed exactly applied to the same space group $P2_1/c$, which is characteristic of the structure of the α2 form. No extra extinction condition was found for those obtained in

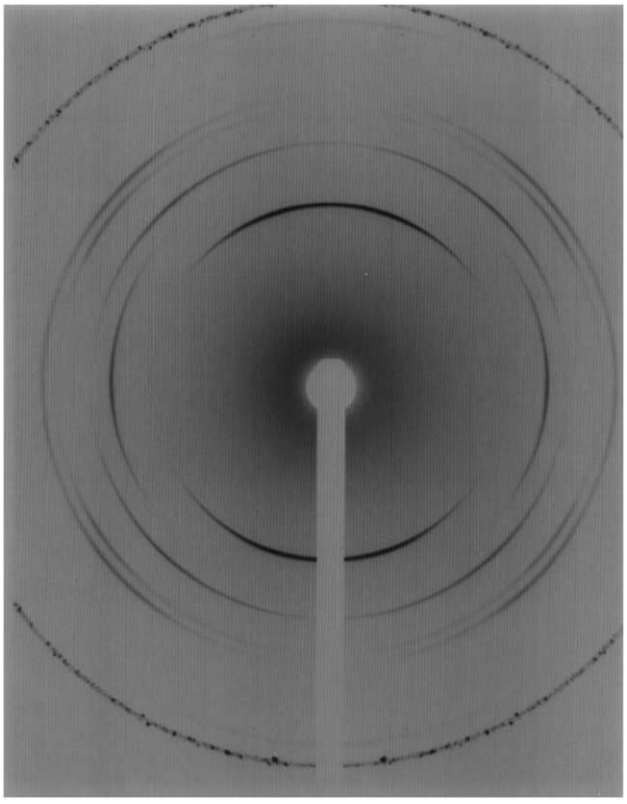

Fig. 3. X-ray diffraction patterns obtained at T_R. A 0.3 mm collimator was used and the sample was rotating along the a^* axis under X-ray radiation (90 kV × 60 mA) for 8 h. Dotted lines indicate 111 reflections from Si powder.

the high temperature region. In this sense, it is safe to conclude that all the X-ray patterns, although obtained at very different annealing temperatures, are substantially identical.

Particularly, it is also worth noting here that the relative intensities of $\bar{1}61$ and $\bar{2}31$ to other reflections are approximately the same in Figs. 5 and 6. This means that the fraction of the α2 form ($f(\alpha 2)$) keeps almost unchanged throughout the whole annealing temperature region. As a matter of fact, it was found by Radhakrishnan et al. that the $f(\alpha 2)$ could approach to unity when the sample ([mmmm] = 99.5%) was crystallized isothermally at high temperature [11]. Since the reflection pattern in this study strongly resembles their published result, we would conclude that the $f(\alpha 2)$ of the sample used in this study (crystallization temperature $T_c = 160$ °C, [mmmm] = 99.6%) has also approached to unity and kept almost constant upon annealing.

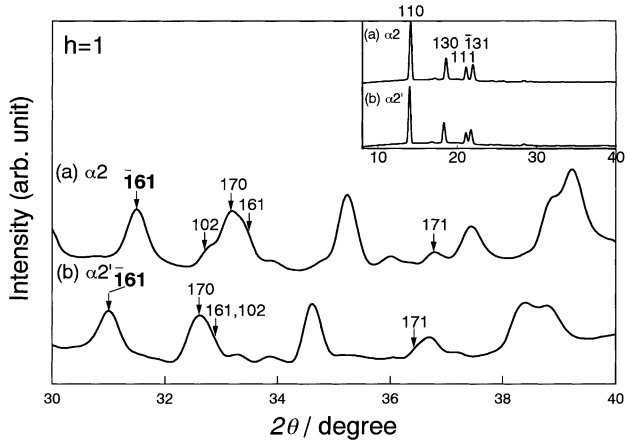

Fig. 5. The observed X-ray fiber pattern ($h = 1$) in the 2θ interval 30–40°. The inserted graph is the whole pattern: (a) annealed at room temperature under X-ray exposure for 8 h, (b) annealed at $T_a = 166$ °C under X-ray exposure for 8 h.

3.3. Lattice spacing

Fig. 7(a) and (b) shows the annealing temperature dependence of the relative changes of the lattice spacing of reflections having indices $hk0$ and $hk1$, respectively.

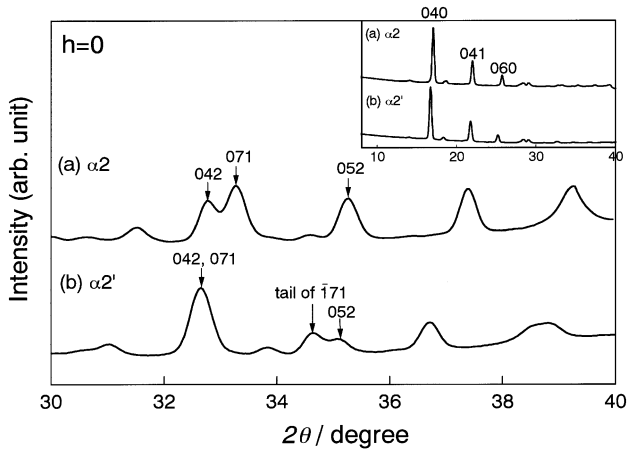

Fig. 4. The observed X-ray fiber pattern ($h = 0$) in the 2θ interval 30–40°. The inserted graph is the whole pattern: (a) annealed at room temperature under X-ray exposure for 8 h, (b) annealed at $T_a = 166$ °C under X-ray exposure for 8 h.

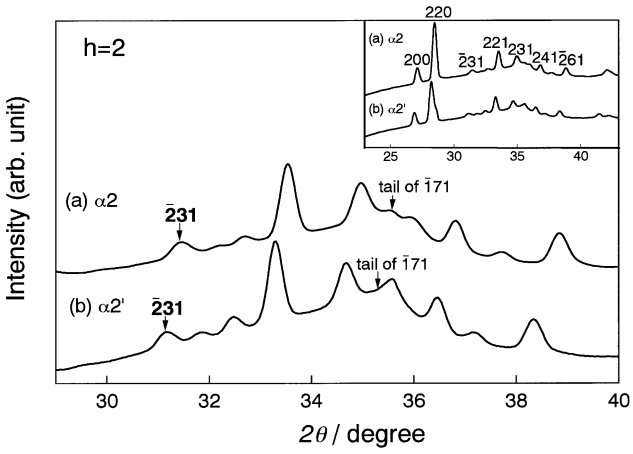

Fig. 6. The observed X-ray fiber pattern ($h = 2$) in the 2θ interval 30–40°. The inserted graph is the whole pattern: (a) annealed at room temperature under X-ray exposure for 8 h, (b) annealed at $T_a = 166$ °C under X-ray exposure for 8 h.

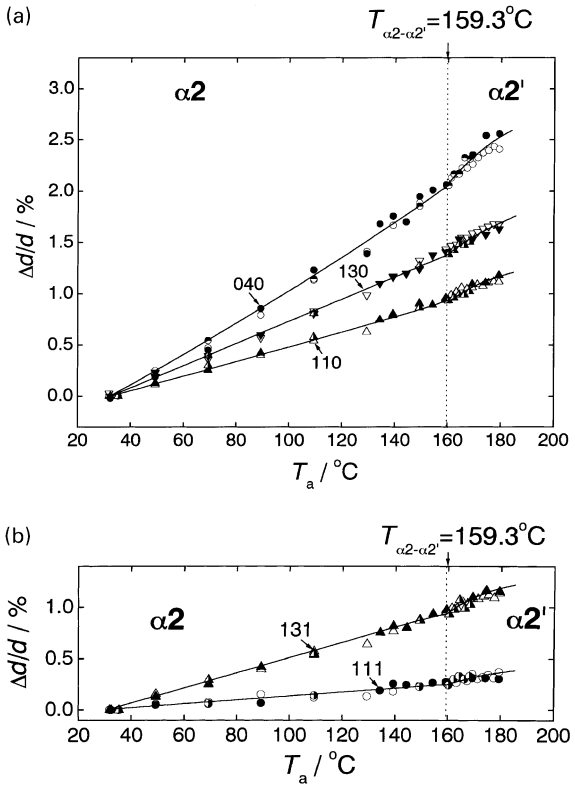

Fig. 7. Temperature dependence of relative changes of lattice spacing $\Delta d/d$ for (a) $hk0$ and (b) for $hk1$ indices on annealing. Different patterns in one symbol indicate independent measurements.

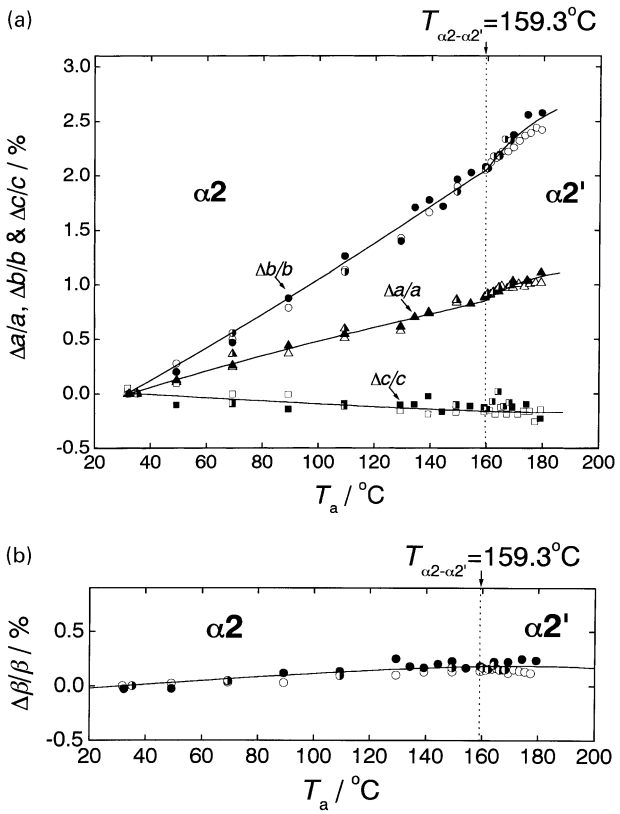

Fig. 8. Temperature dependence of relative changes of lattice constants $\Delta a/a$, $\Delta b/b$, $\Delta c/c$ (a) and $\Delta\beta/\beta$ (b) on annealing. Different patterns in one symbol indicate independent measurements.

Discontinuous increases in the slopes of lattice spacing versus T_a plots were observed at $T_a = 159.3$ °C for all reflections, which indicates the occurrence of a kind of phase transition. Here, we will define the new phase as the $\alpha2'$ form and denote the transition temperature as $T_{\alpha2-\alpha2'}$. In Section 3.5, we will again confirm that such a phase transition is of the second order.

By close observation, we found that the slope changes in the lattice spacing of 110 and 130 reflections are much more evident than those of the 111 and $\bar{1}31$ reflections. Hence, we could speculate that the lattice constants a and b might experience significant changes, whereas c remains almost constant.

When the sample was brought back to room temperature, it was found that all lattice spacing recovered their original values.

3.4. Lattice constants determination

Fig. 8(a) shows temperature dependence of the relative changes of lattice constants on annealing. As expected, both the $\Delta a/a$ and $\Delta b/b$ versus T_a plots show more rapid increase above $T_a = 159.3$ °C. This means that the slopes of the above plots should have discontinuous changes at $T_a = 159.3$ °C. Meanwhile, the $\Delta c/c$ keeps almost constant against T_a.

Fig. 8(b) shows the $\Delta\beta/\beta$ against T_a plot. Similar to the change of the c, the β also experiences no significant change throughout the whole annealing temperature region.

For a more quantitative description, the lattice constants a, b and c against T_a plots were fitted using polynomial equation with $n = 2$. As a result, the linear thermal expansion coefficients can be easily obtained by Eq. (1)

$$\beta_T = \frac{1}{x}\frac{\mathrm{d}x}{\mathrm{d}T}, \tag{1}$$

where x is a lattice parameter. The results were summarized as follows:

$$\begin{cases} \beta_a(\alpha2) = 6.78\times10^{-5}\ \mathrm{K}^{-1} \\ \beta_b(\alpha2) = 1.80\times10^{-4}\ \mathrm{K}^{-1} \\ \beta_c(\alpha2) = -5.62\times10^{-6}\ \mathrm{K}^{-1} \end{cases}$$

for $T_a = T_{\alpha2-\alpha2'} = 159.3$ °C (2a)

and

$$\begin{cases} \beta_a(\alpha2') = 1.37\times10^{-4} \approx 2.0\beta'_a(\alpha2)\ \mathrm{K}^{-1} \\ \beta_b(\alpha2') = 2.70\times10^{-4} \approx 1.5\beta_b(\alpha2)\ \mathrm{K}^{-1} \\ \beta_c(\alpha2') = -5.62\times10^{-6} = \beta_b(\alpha2)\ \mathrm{K}^{-1} \end{cases}$$

for $T_a = T_{\alpha2-\alpha2'} = 159.3$ °C. (2b)

It is seen that the linear thermal coefficients of a and b in the

$\alpha 2'$ phase are significantly larger than those in the $\alpha 2$ phase, whereas the c is just the same. Naturally, one may speculate that molecular chains should gain much more mobility at high temperature due to the significant increase in inter-chain distance.

3.5. Unit cell volume determination and second-order phase transition

Fig. 9 shows the unit cell volume V versus T_a plot. Again, an evidence of more rapid increase above $T_{\alpha 2-\alpha 2'}$ can be discerned, which means a discontinuous change in the slope of V versus T_a plot, i.e.

$$\left(\frac{\partial V}{\partial T}\right)_{p,\alpha 2} \neq \left(\frac{\partial V}{\partial T}\right)_{p,\alpha 2'} \quad \text{at } T = T_{\alpha 2-\alpha 2'}. \tag{3}$$

As a matter of fact, it was found that the volume thermal expansion coefficient of the $\alpha 2$ phase is about 2.8 times larger than the one of the $\alpha 2'$ phase, i.e.

$$\alpha_v(\alpha 2') \approx 2.8\alpha_v(\alpha 2). \tag{4}$$

However, the volume itself changes continuously. This means

$$V_{\alpha 2} = V_{\alpha 2'}. \tag{5}$$

Combining Eqs. (4) and (5), the above change can be proved to be the second-order phase transition [35]. Again, note that the new phase is termed $\alpha 2'$ form in this study.

4. Discussion

4.1. Second-order phase transition from immobile phase to mobile phase

So far we have shown that the unit cell of iPP can expand much more rapidly in the high temperature region of the $\alpha 2'$ phase. It is thus reasonable to suppose that molecular chains would become much more mobile. As a result, the molecular chains are capable of arranging themselves nicely in the crystallographic unit cell. This could give rise to the production of the pure form of the ordered $\alpha 2$ form ($f(\alpha 2) = 1$), which has been indeed observed in the iPP sample with very high isotacticity (= 99.5%) isothermally crystallized above $T_c = 150$ °C [11] and also in the present study.

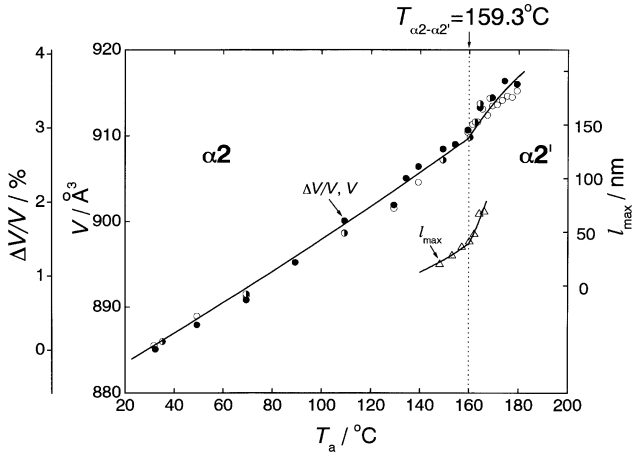

Fig. 9. Temperature dependence of unit cell volume V and maximum lamellar thickness l_{max}. Different patterns in one symbol indicate independent measurements.

Moreover, one may argue that such a second-order phase transition might be closely related to the lamellar thickness and the tacticity. With increase in lamellar thickness and tacticity, the transition temperature $T_{\alpha 2-\alpha 2'}$ would also increase. It is conceivable that the activation energy of mobilization of molecular chains should increase with the perfection of the crystal. Actually, it is an immediate reminiscence to us that the $\alpha 1-\alpha 2$ transition temperature increases with the increase in orientation [4]. As is well known, the effect of orientation will produce more perfect crystals.

Some hints also come from the thermal expansion coefficient measurements on the second heating process. Since the sample was partially melted at very high annealing temperature (~178 °C), some imperfect small crystallites would thus be produced when the sample was brought back to room temperature quickly. Using such a secondly heated sample, we found that the lattice spacing become larger and the transition temperature shifts to the lower temperature region. Such a study essentially constitutes another interesting topic and is now in progress in our laboratory.

4.2. Why lamellae thicken significantly at high temperature?

Following the train of the similar thoughts, one may expect that the better chain sliding diffusion will be promoted after the occurrence of the second-order phase transition. This naturally leads to the acceleration of lamellar thickening within the sample. Actually, we have already shown in the precedent paper that the lamellar thickening rate indeed experiences a sudden increase at very high $T_c \approx$ 157 °C, which should correspond to $T_{\alpha 2-\alpha 2'}$ in the case of the sample having $M_w = 86.4 \times 10^3$ and [mmmm] = 99.5% [34]. In the present paper, a more rapid increase in the maximum lamellar thickness (l_{max}) was again confirmed by transmission electron microscope (TEM) and is shown in Fig. 9.

Furthermore, it is also worth noting that the lamellar thickness distribution becomes much wider in the high temperature region. As a matter of fact, a fairly long tail containing the very thick lamellae content can be seen in the lamellar thickness distribution profile. The existence of these very thick lamellae could give rise to the double melting peaks in the differential scanning calorimetric (DSC) measurements. These exciting results will be reported elsewhere [36].

It was well known that lamellar thickening would possibly take place when polymer crystals were annealed

at a temperature above the crystallization temperature. In case of polyethylene, the lattice constant a also increases significantly at high temperature [37–41]. However, we do not attribute the phenomenon here a resemblance to what happened at high temperature above 80 °C for polyethylene. The α_c relaxation in polyethylene does not result in discontinuous change in volume thermal expansion coefficient and may not induce a much more accelerated lamellar thickening progress.

However, we would again emphasize here that a second-order phase transition takes place simultaneously accompanied by a much faster lamellar thickening process at high temperature sufficiently near to the melting temperature. It is thus fair to conclude that a mobile phase would exist therein. The existence of such a mobile phase is appropriate to account for the extraordinary lamellar thickening process. In this sense, general significance is thus proposed for both semi-crystalline polymer and liquid crystal systems.

4.3. Relationship with melting behavior of high isotactic iPP

Relevant to the observation of the second-order phase transition, we would like to go a little further here and cite the recent results of melting temperature determination on the same sample by Yamada et al. [36]. By means of both the polarizing optical microscope (POM) and DSC measurements, they found that the melting temperature T_ms (including both the T_m(OM) and T_m(DSC)) increase much more rapidly above $T_{\alpha 2-\alpha 2'} = 159.3$ °C. According to the Gibbs–Thomson equation, the melting temperature should have a linear relationship with the inverse of lamellar thickness. Note that the T_m(OM) corresponds to the melting temperature of the thickest lamellae within the crystal, whereas the T_m(DSC) is linked with the whole distribution of lamellar thickness. Also bearing in mind that there exists a fast lamellar thickening process at high temperature [34], it is safe to conclude here that the four independent sets of experiments are closely related and consistent with each other. All of them strongly indicate that the iPP experiences a transition from the immobile phase at lower temperature to the mobile phase at high temperature. As shown in this study, such a transition has been confirmed to be the second-order phase transition by means of X-ray measurement.

5. Conclusions

1. The slopes of lattice constants a and b versus T_a plots increase discontinuously at $T_a = 159.3$ °C. The c and the β, however, remain almost constant throughout the whole annealing temperature region.
2. The slope of unit cell volume V versus T_a plot also shows a discontinuous increase at $T_a = 159.3$ °C, indicating the occurrence of the second-order phase transition.
3. After the occurrence of the second-order phase transition, chain molecules become much more mobile. This could account for the fast lamellar thickening process at high temperature reported in our precedent paper.
4. Both the T_m(OM) and the T_m(DSC) versus T_c plots show more rapid increases in the high temperature region (>159.3 °C). Such an observation again confirms the existence of the mobile phase.

Acknowledgements

The authors gratefully acknowledge the financial support provided by international Joint Research grant, NEDO 1995–1998 and Grant-in-Aid for scientific Research, Scientific Research on Priority Areas, B2 (No. 12127205), Scientific Research A2 (No. 12305062), Scientific Research C2 (No. 11640378) and that for JSPS fellows (No. 98434). The authors are grateful to Dr B. Lotz for valuable suggestions. Thanks go to Rigaku Denki Co., Ltd and Mr Sasaki for cooperation on the development of the 'Fiber Data Processing' software. Thanks also go to Sunallomer Ltd for providing the high isotactic iPP.

References

[1] Natta G, Corradini P. Suppl Nuovo Cimento 1960;15:40.
[2] Norton DR, Keller A. Polymer 1985;26:704.
[3] Mencik Z. J Macromol Sci 1972;6:101.
[4] Hikosaka M, Seto T. Polym J 1973;5:111.
[5] Corradini P, Napolitano R, Oliva L, Petraccone V, Pirozzi B, Guerra G. Makromol Chem, Rapid Commun 1982;3:753.
[6] Corradini P, Petraccone V, Pirozzi B. Eur Polym J 1983;19:299.
[7] Auriemma F, De Ballesteros OR, De Rosa C, Corrandini P. Macromolecules 2000;33:8764.
[8] Cheng SZD, Janimak JJ, Zhang AQ, Hsieh ET. Polymer 1991;32:648.
[9] Janimak JJ, Cheng SZD, Giusti PA, Hsieh ET. Macromolecules 1991;24:2253.
[10] Janimak JJ, Cheng SZD, Zhang AQ, Hsieh ET. Polymer 1992;33:728.
[11] Radhakrishnan J, Ichikawa K, Yamada K, Toda A, Hikosaka M. Polymer 1998;39:2995.
[12] Lotz B, Wittmann JC. J Polym Sci, Polym Phys Ed 1986;24:1541.
[13] Yamada K, Mastumoto S, Tgashira K, Hikosaka M. Polymer 1998;39:5327.
[14] Keith HD, Padden Jr FJ, Walter NM, Wyckoff HW. J Appl Phys 1959;30:1485.
[15] Turner-Jones A, Aizlewood JM, Beckett DR. Makromol Chem 1964;75:134.
[16] Varga J. J Therm Anal 1986;31:165.
[17] Lotz B, Kopp S, Dorset DL. Compt Rend Acad Sci (Paris) SerII b 1994;319:187.
[18] Lovinger AJ, Chua JO, Gryte CC. J Phys E 1976;9:927.
[19] Shi G, Zhang X, Qiu Z. Makromol Chem 1992;193:583.
[20] Morrow DR, Sauter AJ. Nature 1966;211:514.
[21] Hikosaka M, Sato N, Hasegawa M, Seto T. Jpn J Appl Phys 1973;12:1293.
[22] Nakafuku C. Polymer 1981;22:1673.
[23] Lotz B, Graff S, Wittmann JC. J Polym Sci, Polym Phys Ed 1986;24:2017.
[24] Brückner S, Meille SV. Nature 1989;340:455.
[25] Meille SV, Brückner S, Porzio W. Macromolecules 1990;23:4114.
[26] Lotz B, Graff S, Staupe C, Wittmann JC. Polymer 1991;32:2902.
[27] Miller RL. Polymer 1960;1:35.

[28] Addink EJ, Beitema J. Polymer 1961;2:185.
[29] Chandrasekhar S. Liquid crystals. 2nd ed. New York: Cambridge University Press, 1992.
[30] Hikosaka M. In: Teramoto A, Kobayashi M, Norisuye T, editors. Ordering in macromolecular systems. Berlin: Springer, 1994. p. 89–97.
[31] Anderson FR. J Appl Phys 1964;35:64.
[32] Hikosaka M. Polymer 1987;28:1257.
[33] Hikosaka M. Polymer 1990;31:458.
[34] Maiti P, Hikosaka M, Yamada K, Toda A, Gu F. Macromolecules 2000;33:9069.
[35] Laidler KJ, Meiser JH. Physical chemistry. 3rd ed. Boston: Houghton Mifflin, 1999.
[36] Yamada K, Hikosaka M, Toda A, Ghosh SK, Gu F, Yamazaki S, Arakaki M. In preparation.
[37] Cole EA, Holmes DR. J Polym Sci 1960;XLVI(147):245.
[38] Davis GT, Eby RK, Martin GM. J Appl Phys 1968;39(11):4973.
[39] Davis GT, Eby RK, Colson JP. J Appl Phys 1970;41(11):4317.
[40] Kitamaru R, Mandelkern L. J Poym Sci Part A-2 1970;8:2079.
[41] Kawaguchi A, Ichida T, Murakami S, Katayama K. Colloid Polym Sci 1984;262:597.